Available online at www.sciencedirect.com
ScienceDirect
Journal of Solid State Chemistry 180 (2007) 3366–3380
JOURNAL OF SOLID STATE CHEMISTRY
www.elsevier.com/locate/jssc

# Increase of ionic conductivity in the microporous lithosilicate RUB-29 by Na-ion exchange processes

S.-H. Park[a,*], A. Senyshyn[b,c], C. Paulmann[d,e]

[a]*Section Crystallography, Earth and Environmental Sciences, Ludwig-Maximilians-Universität München, Theresienstr. 41, 80333 Munich, Germany*
[b]*Material- and Earth Sciences, Technische Universität Darmstadt, Petersenstr. 23, 64287 Darmstadt, Germany*
[c]*Forschungsneutronenquelle Heinz Maier-Leibnitz (FRM II), Lichtenbergstr. 1, 85747 Garching, Germany*
[d]*Mineralogisch-Petrographisches Institut, Universität Hamburg, Grindelallee 48, 20146 Hamburg, Germany*
[e]*HASYLAB, DESY, Notkestr. 85, 22603 Hamburg, Germany*

Received 14 August 2007; received in revised form 20 September 2007; accepted 21 September 2007
Available online 31 October 2007

**Abstract**

The ionic conductivity in the zeolite-like lithosilicate RUB-29 ($Cs_{14}Li_{24}[Li_{18}Si_{72}O_{172}]\cdot 14H_2O$ [S.-H. Park, J.B. Parise, H. Gies, H. Liu, C.P. Grey, B.H. Toby, J. Am. Chem. Soc. 122 (2000) 11023–11024]) increases via simple ion-exchange processes, in particular when Na cations replace a part of $Cs^+$ and $Li^+$ of the material. The resulting ionic conductivity value of $3.2\times10^{-3}\,S\,cm^{-1}$ at 885 K is about two orders higher than that for the original material [S.-H. Park, J.B. Parise, M.E. Franke, T. Seydel, C. Paulmann, Micropor. Mesopor. Mater., in print (doi:10.1016/j.micromeso.2007.03.040 available online since April 19, 2007)]. The structural basis of a $Na^+$-exchanged RUB-29 sample (Na-RUB-29) at 673 K could be elucidated by means of neutron powder diffraction. Rietveld refinements confirmed the replacement of $Na^+$ for both parts of Cs and Li cations, agreeing with idealized cell content, $Na_8Cs_8Li_{40}Si_{72}O_{172}$. As a result of the incorporation of $Na^+$ in large pores, the number of $Li^+$ vacancies in dense $Li_2O$-layers of the structure could increase. This can be one of the main reasons for the improved conductivity in Na-RUB-29. In addition, mobile Na cations may also contribute to the conductivity in Na-RUB-29 as continuous scattering length densities were found around the sites for Na in difference Fourier map.
© 2007 Elsevier Inc. All rights reserved.

*Keywords:* Ionic conductivity; Lithosilicate; RUB-29; Na-RUB-29; Ion-exchange; Lithium; Neutron diffraction; Impedance; Rietveld refinement

## 1. Introduction

Based on the high Li mobility [1] and thermal stability up to 1073 K [1,2], the zeolitic lithosilicate RUB-29 ($Cs_{14}Li_{24}[Li_{18}Si_{72}O_{172}]\cdot 14H_2O$) stands as an interesting object for further investigation. In particular, the material is considered as a new type Li-conductor due to a high amount of Li cations in both framework and extraframework. The former ones build up $Li_2O$-layers of edge-sharing $LiO_4$-/$LiO_3$-moieties in its microporous framework [1]. Among zeolites and microporous ionic conductor materials only a couple of lithosilicates [1,3] display such $Li_2O$-layer-containing framework. The microporosity of RUB-29 is ensured by the presence of 10-/8-membered ring (MR)-channels of $SiO_4$-tetrahedra. The alternating stacks of microporous $SiO_2$-sheets and densely packed $Li_2O$-layers are interconnected parallel to the crystallographic *c*-axis, resulting in the framework structure of RUB-29. Additional extraframework Li and Cs cations disordered along with water molecules reside in its micropore system providing additional pathways for conducting Li, being unique from other well-known dense Li-ionic conductor Li-silicates and -oxides.

Although variable-temperature $^7$Li MAS NMR spectroscopy revealed a high degree of Li local mobility in RUB-29 [1], a moderate direct current (DC) conductivity value of $2–6\times10^{-5}\,S\,cm^{-1}$ at 873 K was obtained from impedance spectra of dehydrated RUB-29 [2]. Our previous high-resolution neutron powder diffraction (HRNPD) study

*Corresponding author. Sektion Kristallographie, Geo- und Umweltwisseschaften der LMU, Theresienstr., 41, 80333 München, Germany. Fax: +49 89 289 14015.
*E-mail address:* sohyun.park@lmu.de (S.-H. Park).

0022-4596/$ - see front matter © 2007 Elsevier Inc. All rights reserved.
doi:10.1016/j.jssc.2007.09.026

showed that all non-framework Li cations (8 per unit cell) migrate from the pore system into the framework $Li_2O$-layers after the water loss above 473 K [2]. As a result of the migration, the decrease of the number of unoccupied sites within the $Li_2O$-layers was observed, which could impede the improvement of Li-ionic conductivity at elevated temperatures.

When the amount of Li vacancies or interstitials in the $Li_2O$-layers of RUB-29 is high enough, this can stimulate $Li^+$ hopping in such a layer-like configuration formed by edge- and corner-sharing $LiO_4$-tetrahedra [1,2]. In order to increase the number of those defect sites in RUB-29, isomorphic substitution of multivalent cations for a portion of framework $Li^+$ has been tried via hydrothermal synthesis. However, synthesis conditions for obtaining such metal-substituted RUB-29-type materials should be still optimized under the circumstance that RUB-29 crystallizes from extremely highly basic starting solutions [4]. Under these conditions, the multivalent metal ions $Mg^{2+}$, $Zn^{2+}$, and $Zr^{4+}$ (they were chosen due to their similar ionic radii to that of $Li^+$ (~0.60 Å) for four-fold coordination with oxygens in silicates and oxides [5]) crystallize readily in their stable hydroxide or oxide forms. Our attempts in hydrothermal syntheses have resulted neither in single phase samples of desired metal-substituted RUB-29 modifications, nor in several mm-sized large single crystals required for further conductivity measurements, up to now.

As another option, taking advantage of a zeolite-like capability of RUB-29, 'simple' ion-exchange processes were chosen to replace $Na^+$ or $Mg^{2+}$ for its extraframework $Cs^+$ and $Li^+$, or to incorporate more $Li^+$ in its channels. Li-dynamics in dehydrated forms of several ion-exchanged RUB-29 variants were studied using alternating current (AC) impedance spectroscopy (IS), where the temperature dependence of the overall dielectric response was determined for $Na^+$-, $Mg^{2+}$- and $Li^+$-exchanged RUB-29 materials (idealized structural unit content: $Cs_6Na_{10}Li_{40}Si_{72}O_{172}$, $Cs_{12}Mg_{1.5}Li_{41}Si_{72}O_{172}$, and $Cs_9Li_{47}Si_{72}O_{172}$, respectively) [6]. Among these three modifications only the $Na^+$-exchanged RUB-29 showed a higher ionic conductivity. Once RUB-29 is $Na^+$-exchanged, the conductivity reached a value of $7 \times 10^{-3}$ S cm$^{-1}$ at 873 K which is two-orders higher than that in RUB-29 [2,6]. In contrast, relatively lower ionic conductivity values of $1 \times 10^{-5}$ and $2 \times 10^{-6}$ S cm$^{-1}$ at 873 K were observed for both $Mg^{2+}$- and $Li^+$-exchanged samples, respectively. Based on that, one can predict that the configuration of extraframework constituents may sufficiently influence the bulk conductivity in RUB-29-type materials. The present study is aimed to explain the structural reason for the improved ionic conductivity in $Na^+$-exchanged RUB-29.

On the other hand, our on-going synchrotron X-ray single crystal diffraction (XSD) studies on the structural ordering in RUB-29 have shown that both hydrated (as-synthesized) and dehydrated forms of RUB-29 exhibit one-dimensional incommensurably modulated superstructures in superspace group symmetry $\boldsymbol{I}222(\alpha 00)000$ below and at room temperature [7]. Structural modulation seems to be degraded by zeolitic water molecules, as hydrated RUB-29 gives rise to no satellite reflections more at room temperature. Furthermore, below room temperature, relative intensities of satellite reflections with respect to main reflections of hydrated RUB-29 are weaker than those from dehydrated RUB-29. At temperatures above 473 K, superstructure reflections of dehydrated RUB-29 disappear [2]. High-temperature form of RUB-29 possesses the same prototype space group symmetry $\boldsymbol{I}222$ as its basic structure (as-synthesized) [2]. In the current report, concerning these superstructure problems, we deal with the structure of a high-temperature form of dehydrated Na-RUB-29 at 673 K in connection with its high ionic conductivity which cannot be affected from the temperature-induced structural modulation and the water molecules. This will be further discussed to seek contrast to dehydrated RUB-29 in order to unveil the consequences of $Na^+$ incorporation into RUB-29.

## 2. Experimental

### 2.1. Na-ion exchange processes

Optimized synthesis parameters for fine crystallites of pure RUB-29, as well as those for its large crystals (edge-length up to 150 μm) were reported in [1,2,4]. The $Na^+$-exchanged RUB-29 sample in the previous IS study [6] mentioned above was obtained by three times repetition of a 2-h ion-exchange process. For collecting HRNPD and IS data in this study, each single step of $Na^+$-exchanging tasks was performed in a shorter time in order to ensure a less hydrolyzed sample after ion-exchanging, as follows: 3 g powder of a batch RUB-29 sample was contacted to 200 ml of a 1 mol NaCl solution for about 30 min in slowly stirring. This was washed with a plenty amount of deionized water until the solution showed a pH value of 7–8. The filtered sample was dried at room temperature before the ion-exchanging procedure was repeated with a less concentrated 0.7 mol NaCl solution. The third Na-exchanging step was performed in 100 ml of a 0.5 mol NaCl solution made with $D_2O$. The use of heavy water is to minimize the incoherent scatter due to protons in neutron powder diffraction. The final $Na^+$-exchanged sample was washed also with heavy water and kept in a drying oven at 473 K until the collecting of HRNPD data.

For collecting XSD data, 80–150 μm-sized crystals of RUB-29 were contacted to a 1 mol NaCl solution in slowly stirring. The solution was refreshed twice within 22 h, and then the crystals were washed with deionized water and dried at room temperature.

### 2.2. Impedance spectroscopy

To validate the high conductivity in Na-RUB-29 [6], a new series of IS spectra was acquired with the $Na^+$-exchanged RUB-29 sample prepared in this study. A pellet

(diameter = 3 mm and thickness = 2 mm) was made with the sample, and both its ends were covered with Pt-paint and then clamped between Pt-plates. The complex impedance $Z^*(\nu)$ was recorded with a Hewlett Packard LCR meter (4284A) in the frequency range 20–$10^6$ Hz. A NiCr-Ni thermocouple was located close to the sample (~0.3 mm distance), and the sample temperature was maintained to be stable ($\pm$0.3 K) using a temperature controller. The measuring chamber was under $N_2$ (99.999%) atmosphere throughout the whole experiments.

After the pellet was dehydrated within the measuring cell at 473 K overnight, electrical linearity of the sample response was probed in 1 V. The IS spectra were recorded twice upon heating and cooling between 473 and 943 K at intervals of 30 K. The second measurement was performed with the identical pellet and settings directly after the first run.

In our former investigation, two sets of IS spectra of dehydrated RUB-29 samples were obtained at two different institutes (RWTH Aachen and LMU München, Germany) [2,6], and, based on the evaluated bulk conductivity (Table 1), the structural basis for Li-dynamics was reported [2]. In the present work, the set of IS spectra, which were obtained at LMU under the same measuring condition for acquiring IS spectra with the Na-RUB-29 sample described above, will be presented in more detail in order to figure out differences in charge transfer processes in RUB-29 before and after $Na^+$ incorporation.

### 2.3. Synchrotron X-ray single crystal diffraction

To ensure the absence of temperature- and dehydration-induced superstructure of high-temperature forms of Na-RUB-29, a set of XSD data was collected at 473 K on a KAPPA-diffractometer at the instrument F1 (Hamburger Synchrotronstrahlungslabor). A plate-like crystal of Na-RUB-29 (edge-length of ~50 μm) was affixed using epoxy glue onto the sharpened tip of a 0.1 mm diameter glass capillary. For monitoring the dehydration process, initially, *in situ* data collection was carried out with 20–30 snap-shots at constant $\varphi$ ( = 1.0° and 1.5°) while increasing the temperature from 293 up to 473 K using a nitrogen gas stream oven. The measurement of XSD data was subsequently performed at 473 K in $\varphi$-scan mode from 1° to 361° in steps of 0.5°($\Delta\varphi$) with wavelength $\lambda = 0.7100(3)$ Å using a Si(111) monochromator. Intensities were registered with a CCD camera (marCCD 165) positioned at 60 mm from the crystal. The set of XSD data was indexed and integrated using the program package XDS [8] and reciprocal lattice planes were reconstructed using the software XCAVATE [9].

### 2.4. Neutron powder diffraction

Prior to collecting HRNPD data, 2 g of $Na^+$-exchanged, deuterated RUB-29 powder sample was packed in a Nb-cuvette and heated at 473 K for 2 h in a high-temperature Nb vacuum furnace set at the instrument SPODI at FRM II. Data collection was performed at 674 K in a $2\theta$-range of 0–160° in steps of 0.05° with a constant wavelength of 1.549 Å (551 reflection of Ge monochromator at 155° take-off angle). About 2-h data acquisition was repeated six times to check the stability of the sample, and these data sets were then merged in order to improve the counting statistics for subsequent structure analysis. Rietveld refinements were carried out using the program package GSAS [10].

## 3. Results and discussion

### 3.1. Impedance spectroscopy

Argand plots of the real part $Z'$ against the imaginary part $Z''$ of complex impedance at various temperatures show semicircles with a low-frequency tail (Figs. 1a–h). The low-frequency tail, which is clearly seen in Figs. 1g–h,

Table 1
Activation energies ($E_a$) and bulk DC conductivity values ($\sigma$) of dehydrated forms of RUB-29 and $Na^+$-exchanged RUB-29 materials evaluated from their IS spectra

| | RUB-29 $Cs_{14}Li_{42}Si_{72}O_{172}$ | Na-exchanged RUB-29[a] $Cs_6Na_{10}Li_{40}Si_{72}O_{172}$[b] | Na-exchanged RUB-29 $Cs_8Na_8Li_{40}Si_{72}O_{172}$ |
|---|---|---|---|
| HF′ | 0.20(1) eV at 313–453 K<br>0.15(1) eV at 473–613 K<br>0.31(3) eV at 633–673 K<br>0.66(2) eV at 693–923 K | Too high to be determined | Too high to be determined |
| HF | 0.53–61 eV at 373–483 K[a]<br>0.97(1) eV at 553–923 K | 0.20 eV at 373–443 K[a]<br>1.22 eV at 473–653 K[a] | 1.45(3) eV at 543–733 K<br>1.04(3) eV at 763–943 K |
| LF | Shoulder | Shoulder | Shoulder |
| LF′ | Not observed | Not observed | 1.18(5) eV at 763–943 K |
| $\sigma$ | $2\sim6\cdot10^{-5}$ S cm$^{-1}$ at 873 K[a] | $7\cdot10^{-3}$ S cm$^{-1}$ at 873 K[a] | $3.2\cdot10^{-3}$ S cm$^{-1}$ at 885 K |

Several relaxation processes could be resolved at very high (HF′), high (HF), low (LF) and very low (LF′) frequency regions.
[a]Reported in [2,6].
[b]The Na content is somewhat higher than that in the Na-ion exchanged RUB-29 sample made in the present study. The difference is due to the differences in both ion-exchange processes (see Section 2).

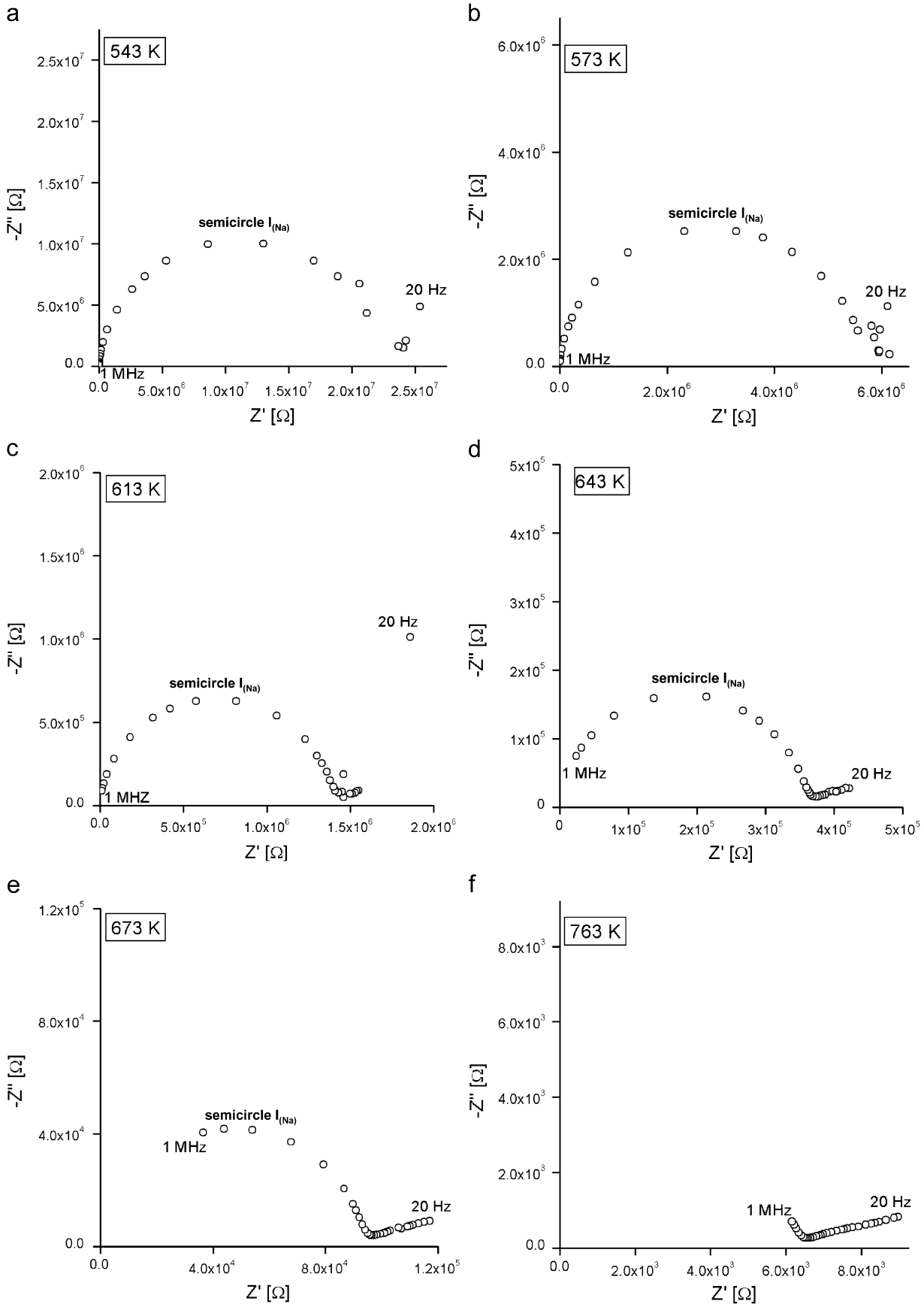


Fig. 1. Impedance spectra of dehydrated Na-RUB-29 ($Cs_8Na_8Li_{40}Si_{72}O_{172}$) acquired during cooling cycle at 543 K (a), 573 K (b), 613 K (c), 643 K (d), 673 K (e), 763 K (f), 853 K (g), and 943 K (h).

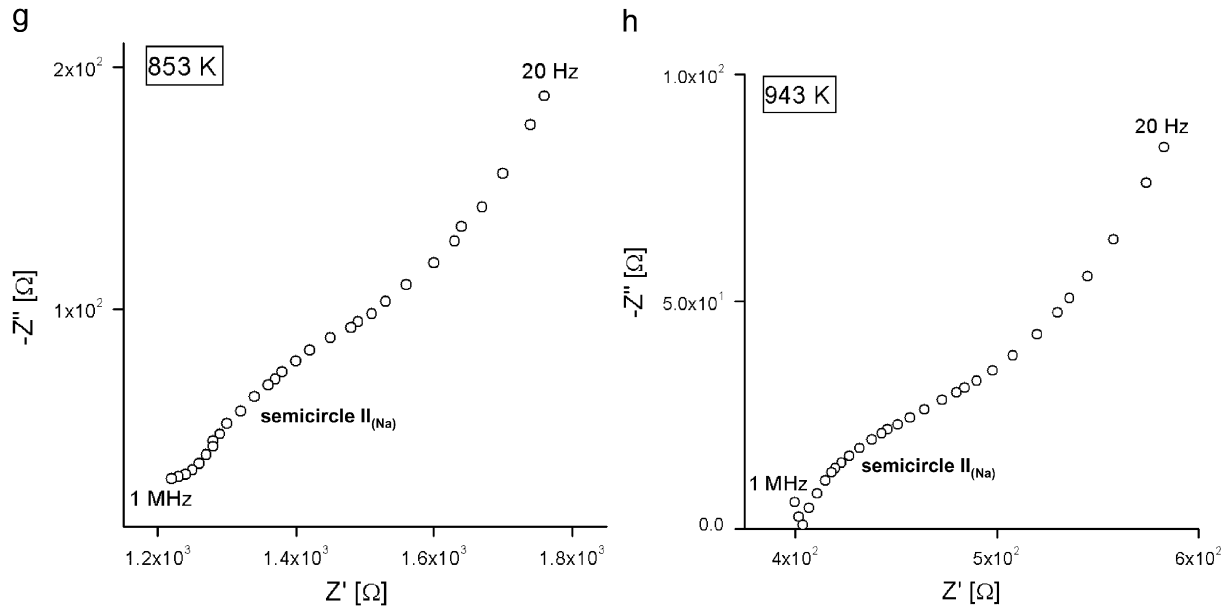


Fig. 1. (*Continued*)

is due to the polarization of the sample/electrode interface and hence indicative of ionic conduction in Na-RUB-29 [11]. Between 543 and 643 K (Figs. 1a–d), a dominant single depressed arc can be seen in the high-frequency (HF) area (denoted as semicircle $I_{(Na)}$, where the subscript $_{(Na)}$ stands for Na-RUB-29). At 493 K, there is a sign of other relaxation processes in the higher-frequency range near 1 MHz (denoted as HF′), but this is too noisy, compared to IS spectra of RUB-29 (see below), to state certain fast motions in the material. A semicircle arises from at least one relaxation process, and the depressed form of a semicircle indicates variations of relaxation time [12]. The size of semicircle $I_{(Na)}$ remained almost constant over the twice repeated cycles of heating and cooling. Therefore, the semicircle $I_{(Na)}$ can be attributed to intraparticle charge transfer processes. The shoulder of semicircle $I_{(Na)}$ in the lower-frequency (LF) region was visible in the first heating cycle, but poorly resolved in the following cooling cycle, as having shifted into the HF region. This can be a trace of sintering effect usually observed in a pellet of powder sample, and hence the LF relaxation process reflects interparticle charge transfer [11,12]. In agreement with the previous IS reports [2,6], the semicircle $I_{(Na)}$ can be assigned to the overall ionic conduction in Na-RUB-29. The decreasing diameter of semicircle $I_{(Na)}$ with increasing temperature (Figs. 1a–e) points to thermally activated processes. Accordingly, with increasing temperature the semicircle $I_{(Na)}$ shifted towards higher frequencies (Figs. 1a–e) and started to move out of the probe frequency window at 763 K (Fig. 1f).

Above 853 K, an incomplete arc (semicircle $II_{(Na)}$ in Figs. 1g–h) appeared at lower frequencies (denoted as LF′). Its curvature increased at elevated temperatures, indicating a decrease in the size of semicircle $II_{(Na)}$. This LF′ relaxation process appeared only in Na-RUB-29 and therefore can be related to slow $Na^+$ motions activated merely above 853 K. However, an unambiguous assignment of the LF′ resonance is not possible, at present.

Apart from difficulties in the assignment of these different relaxation processes to certain mobile Li, Na, and Cs cations, we are now confident that charge transports in dehydrated Na-RUB-29 between 473 and 943 K occur in at least three relaxation processes with distinctive time scales. Other complementary studies such as $^6$Li MAS NMR and quasi-elastic neutron backscattering spectroscopy have been also not easy with resolving variously possible Li motions in RUB-29-type materials [2]. In this situation, for the assignment it is worth seeking contrast of IS spectra of water free Na-RUB-29 to those of RUB-29. This is particularly true for the assignment of the HF′ relaxation processes which could be resolved only in IS spectra of RUB-29 over a wide temperature range of 313–873 K, as semicircle I is seen in Figs. 2a and b. This is more clearly demonstrated by plotting the imaginary parts of impedance ($Z''$) against the logarithm of frequency for each measuring temperature in Figs. 3 and 4 which present temperature-dependence of relaxation frequencies $\nu$ for dehydrated RUB-29 and Na-RUB-29, respectively: $\nu$(HF′) for RUB-29 is visible up to 873 K (Figs. 3a–c), while $\nu$(HF′) for Na-RUB-29 moves out of the measuring frequency window already above 543 K (Fig. 4a). Probably its relaxation time is too fast to be resolved in Na-RUB-29 above 543 K, and $Na^+$-exchange can enormously help to enhance fast cationic motions in the RUB-29 topology.

In addition, the other lower relaxation frequencies $\nu$(HF) and $\nu$(LF) in Na-RUB-29 are also higher than those in RUB-29 (Figs. 3 and 4), reflecting higher overall conductivity in dehydrated Na-RUB-29. The magnitude of DC conductivity ($\sigma$) was obtained by extrapolating $Z''$ of the semicircles due to the respective HF relaxations for $\omega/2\pi \rightarrow$

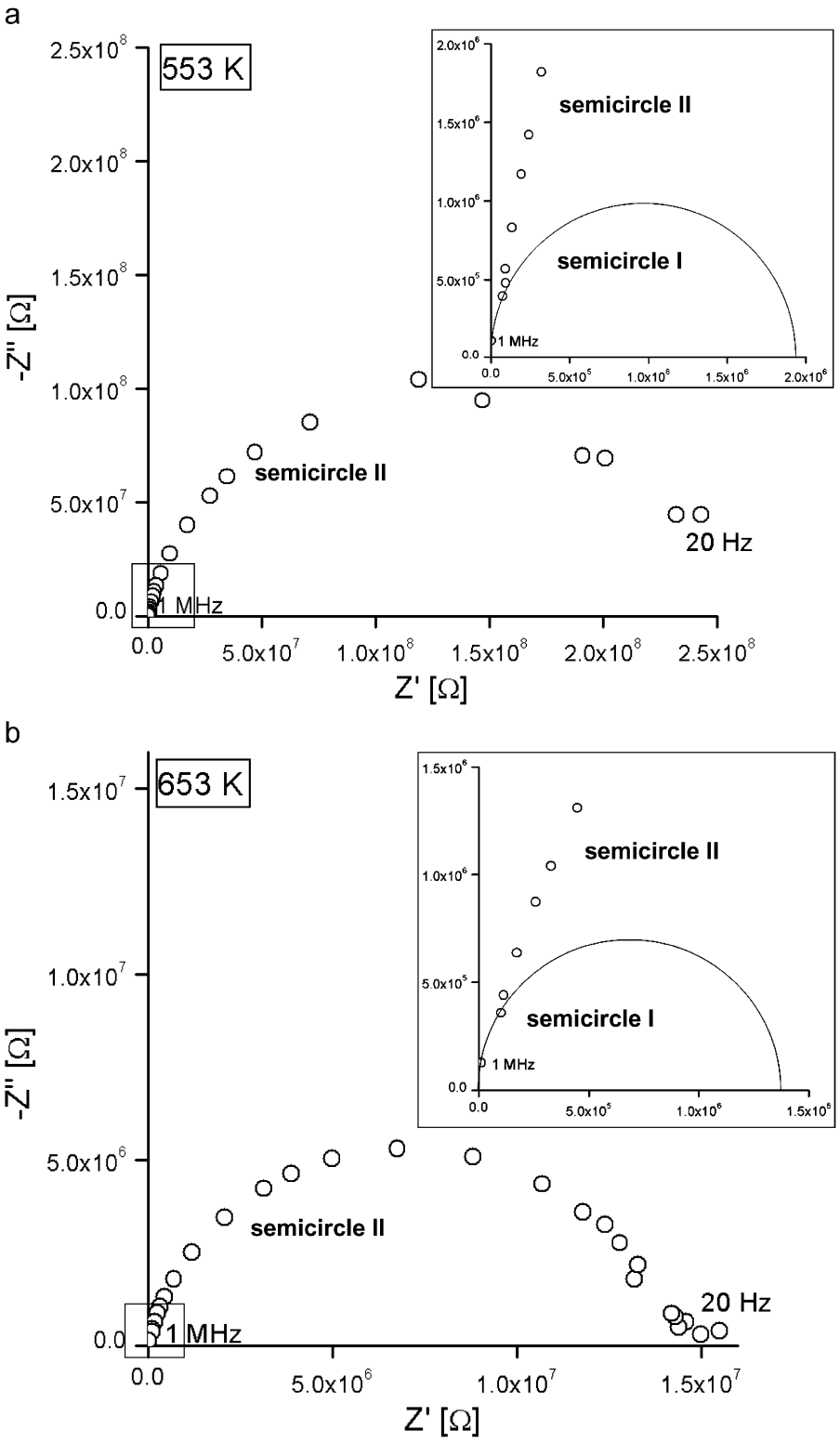


Fig. 2. Impedance spectra of dehydrated RUB-29 ($Cs_{14}Li_{42}Si_{72}O_{172}$) at 553 K (a) and 653 K (b). The insets indicate the presence of semicircle I arising from very high-frequency relaxation processes near 1 MHz.

$\infty$ onto the $Z'$-axis towards the low-frequency side on the impedance plane [13]. In this study, a DC conductivity value of $3.2 \times 10^{-3}\,S\,cm^{-1}$ at 885 K was obtained, confirming the high overall conductivity of Na-exchanged RUB-29 samples observed in the previous IS studies (Table 1).

Compared to the temperature-dependent shifts of $\nu$(HF) and $\nu$(LF), the magnitude of $\nu$(HF′) is constantly high over the investigation temperature range, as there is only a small change of $\nu$(HF′) at elevated temperatures in Figs. 3b–c. Through resolving these HF′ relaxations in dehydrated

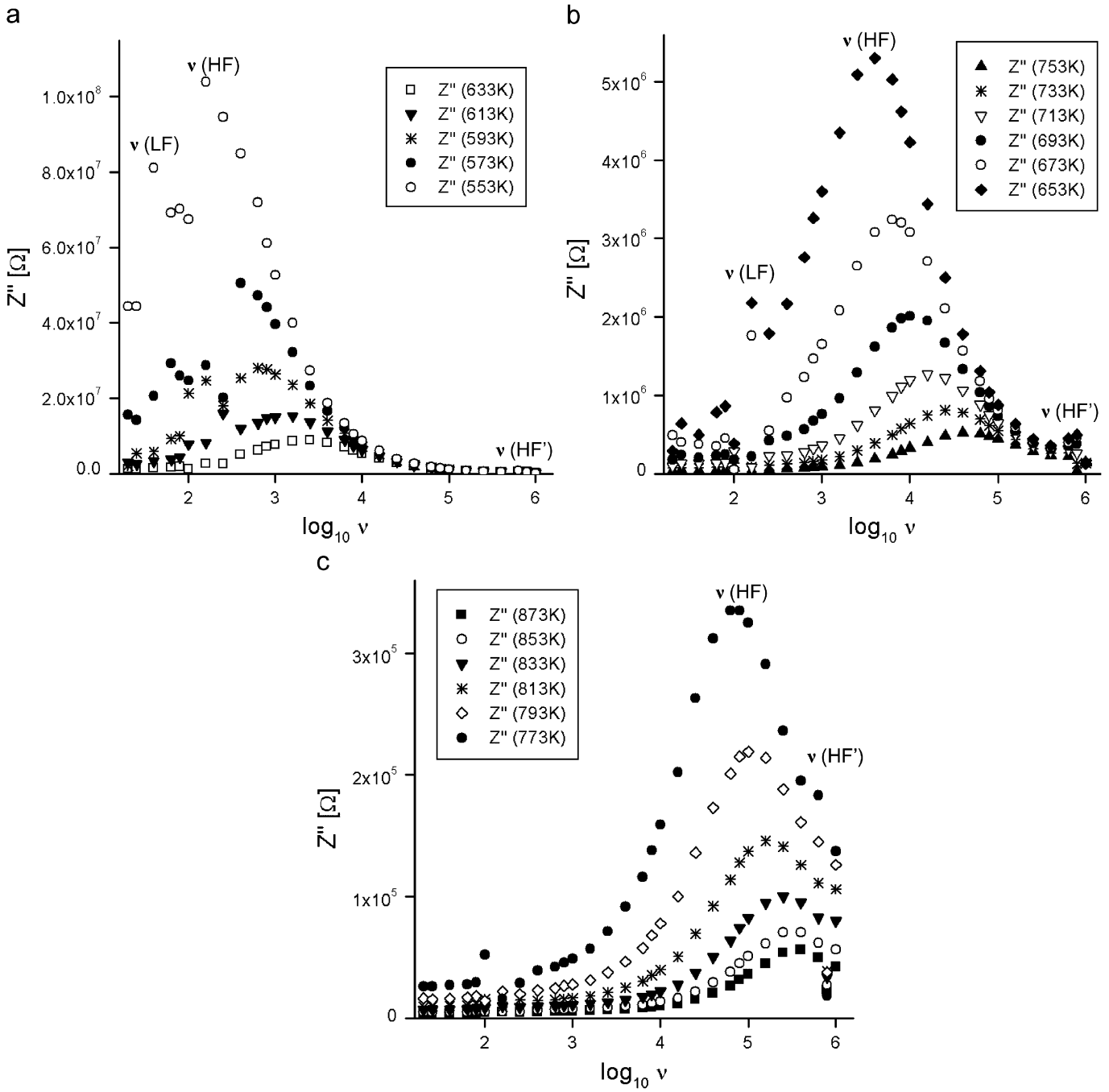


Fig. 3. Plots of imaginary parts $Z''$ of impedance against $\log_{10} v$ ($v$ = AC frequency) for dehydrated RUB-29. Over three different temperature ranges (a)–(c), three-frequency resonances are visible: $v$(LF), $v$(HF), and $v$(HF′) represent low, high, and very high relaxation frequencies, respectively. Both $v$(LF) and $v$(HF) shifted towards higher frequencies with increasing temperature, whereas $v$(HF′) almost unchanged its frequency range up to 873 K.

RUB-29 we do not doubt about results from $^7$Li MAS NMR spectroscopy which showed a high degree of $Li^+$ motions in RUB-29 (4–5 kHz at 473 K [1]). Their site-exchange rates are much higher than that for the overall ionic conduction. Furthermore, it is unlikely that fast Na-cationic motions contribute to high-frequency relaxation processes in Na-RUB-29 alone.

By means of an "Arrhenius-plot", where the obtained values of $\sigma T$ for each measuring temperature are plotted logarithmically against $1/T$, activation energies ($E_a$) for charge transfer processes were estimated (Figs. 5 and 6). The HF′ motions are involved in several different charge transfer processes in RUB-29, as shown in Fig. 5. Below 673 K, only low energy of 0.15(1)–0.31(3) eV was required to activate the HF′ relaxation processes, but the activation energy increases to be 0.66(2) eV at the higher-temperature region above 673 K. A relative high DC conductivity value of $\sigma = 1.2 \times 10^{-6}\,\mathrm{S\,cm^{-1}}$ was evaluated with the HF′ relaxation process in dehydrated RUB-29 at 473 K from the cooling IS runs. Concerning this, attention can be paid

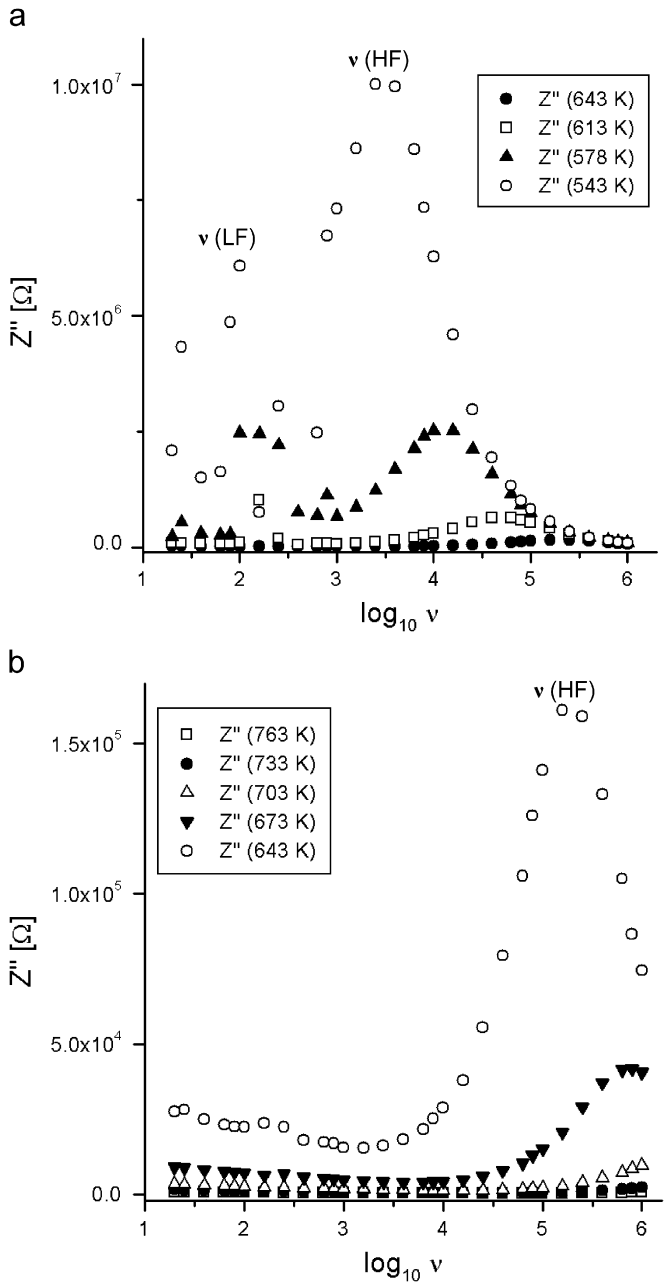


Fig. 4. Plots of imaginary parts $Z''$ of impedance against $\log_{10}\nu$ for dehydrated Na-RUB-29. In a temperature range of 543–763 K two resonance frequencies $\nu$(LF) and $\nu$(HF) could be resolved. At elevated temperatures, both $\nu$(LF) and $\nu$(HF) shifted much faster to higher frequencies (a) with respect to the case of dehydrated RUB-29 (see Fig. 3), and already moved out of the measuring frequency region (b) above 673 K.

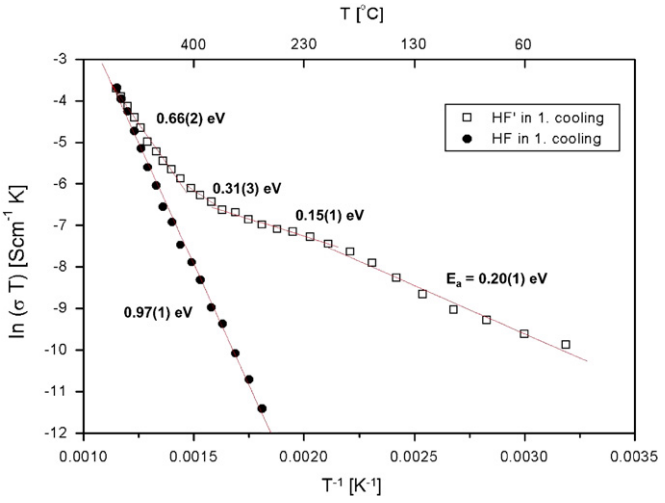


Fig. 5. Arrhenius plot of DC conductivity $\sigma$ estimated from impedance spectra of dehydrated RUB-29 by linear fit $\ln(\sigma T)$ against $1/T$. Several, differently low activation energies ($E_a$) determined for the HF′ motion indicate the presence of various, fast charge transfer processes.

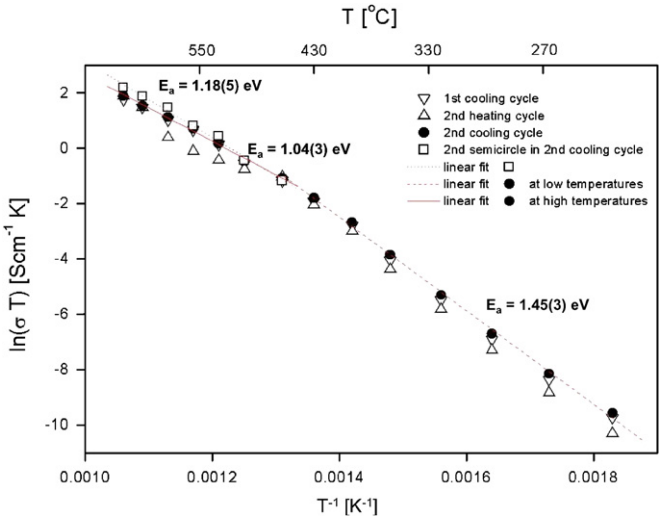


Fig. 6. Arrhenius plot of DC conductivity for dehydrated Na-RUB-29, based on its impedance spectra from twice repeated heating and cooling cycles. With respect to the case of dehydrated RUB-29, at high temperatures above 543 K, the high-frequency relaxation processes in Na-RUB-29 require higher-activation energies of 1.45(3) and 1.04(3) eV (see the main text). At high temperatures above 853 K, a slow motion occurred at the expense of 1.18(5) eV.

to the fact that the same order of magnitude for the conductivity $\sim 10^{-6}\,\mathrm{S\,cm^{-1}}$ at 473 K was estimated in the previous study using variable-temperature $^7$Li MAS NMR spectroscopy [1]. As the latter resulted exclusively from the mobility of one species, i.e. $^7$Li, it is very likely that one of the HF′ relaxation processes is due to fast $Li^+$ motions in dehydrated RUB-29. These highly mobile Li-cations seem to be localized below 673 K (based on the low values of $E_a$), but, above this temperature, migrate over the lattice. On the other hand, localized motions of the Cs cations within relatively narrow 8-/10MR-channels of RUB-29 can be also related with the HF′ relaxation processes. This is based on observations that relative low activation energies are needed for charge transfer processes by $Cs^+$ when they are located within inaccessible cages of zeolitic materials. Therein, bulky $Cs^+$ is only limited to long-range motions requiring higher-energy barrier [11,14].

Compared to these HF′ relaxation processes in RUB-29, the HF motion between 553 and 923 K requires much

higher activation energy, $E_a = 0.97(1)$ eV (Fig. 5, Table 1). However, for this relaxation process at lower temperatures between 373 and 483 K lower activation energy $E_a = 0.53$–$0.61$ eV was determined in the previous study [2,6] (Table 1). With increasing temperature, the hopping rate of the HF motion approaches to that of the HF′ (Fig. 3c). Hence, the HF relaxation process seems to be highly correlated to slow long-range motions of $Li^+$.

In the case of Na-RUB-29, higher-energy barrier $E_a = 1.45(3)$ eV is required for the HF relaxation process between 543 and 733 K (Fig. 6, Table 1). The previous IS study showed a similar high activation between 473 and 653 K (Table 1). At high temperatures above 763 K, the HF relaxation process of Na-RUB-29 demands activation energy of 1.04 (3) eV similar to that in RUB-29. In addition, the energy barrier for the LF′ relaxation process of Na-RUB-29, resulting in semicircle $II_{(Na)}$ in Figs. 1g–h, is also high ( = 1.18(5) eV in Fig. 6). These high activation energies can be addressed to a steric effect of the presence of various types of charge carriers [11,15]. In contrast, at lower temperatures between 373 and 443 K, the HF motion in Na-RUB-29 requires a pretty low-energy barrier of 0.2 eV (Table 1). The bulk conductivity values given in Table 1 are estimated with the semicircles due to the HF relaxation processes.

Although alone using IS spectroscopy it is limited to characterize diverse short- and long-range charge transports in Na-RUB-29, we can here draw a conclusion that the presence of $Na^+$ in RUB-29 causes not only the improvement of the overall conductivity up to two orders of magnitude, but also promotes much faster cationic dynamics. Basically, both fast $Li^+$ and $Cs^+$ motions can contribute to those HF′ relaxation processes in dehydrated RUB-29, as mentioned above. The refined structure of Na-RUB-29 compared with RUB-29 allowed a more confident conclusion, as will be described in the following sections.

### 3.2. Synchrotron X-ray single crystal diffraction

Reconstructed reciprocal planes of the collected XSD data at 473 K show exclusively main reflections which can be indexed in space group *I*222 with cell dimensions of approximately $11 \times 17 \times 24$ Å$^3$ (Fig. 7a), i.e. the basic cell of as-synthesized RUB-29 [1]. However, most main reflections are severely affected by additional reflections in 0th and higher-order planes of the [100] zone (Fig. 7b). They appear around each of intrinsic main reflections in $\omega$-direction of the diffractometer. Hence, those extrinsic reflections are unambiguously regarded as originating from several individual grains intergrown with common crystallographic *a*-axis. It was therefore difficult to integrate intensities properly, and, as a consequence, the quality of the obtained model from the XSD data was low. Therefore, we refrain from reporting the resulting model here and deal only with the refined structure of Na-RUB-29 with HRNPD data at 673 K (cf. the next section). Nonetheless,

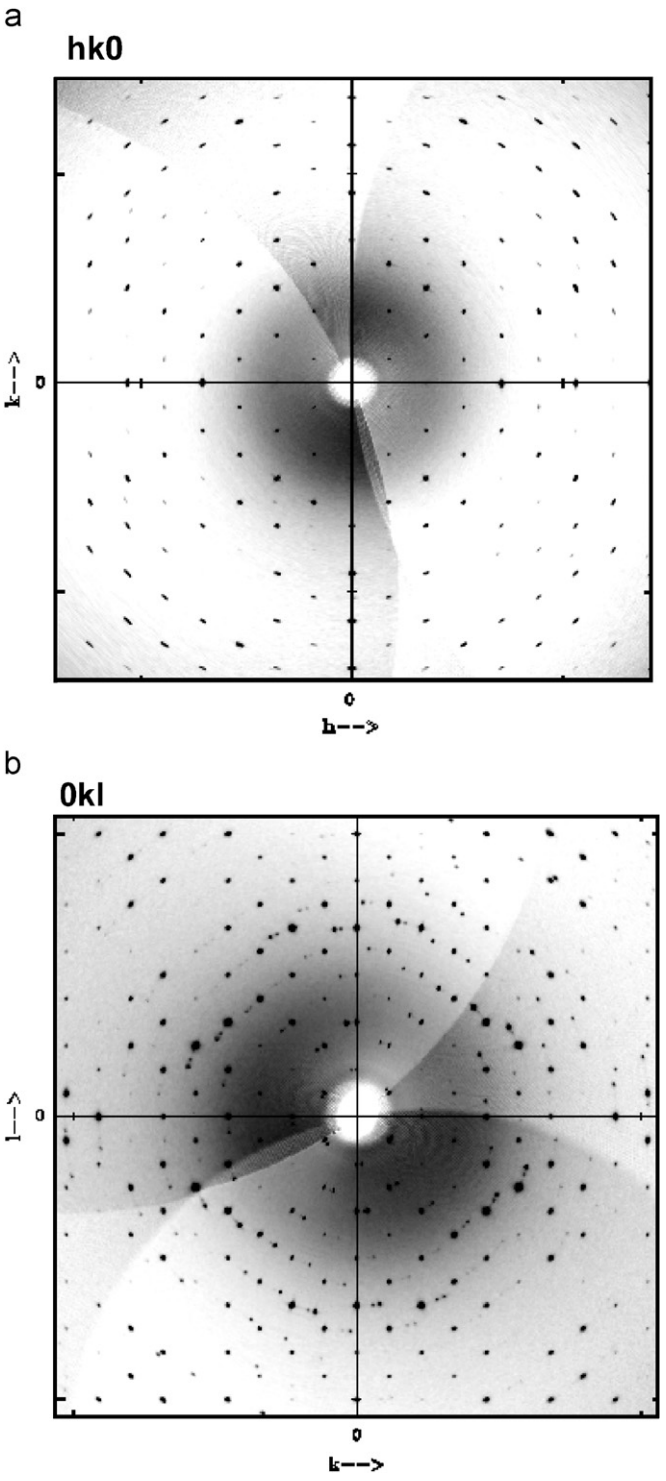


Fig. 7. Reconstructed reciprocal $h\,k\,0$ (a) and $0\,k\,l$ (b) planes of XSD data of dehydrated Na-RUB-29 at 473 K. There is no indication of superstructure reflections (a), but there are many of extra reflections from intergrown grains (b).

the reconstruction of XSD data collected at 473 K was a crucial point in this study, as allowing us a starting model for the performance of Rietveld analysis on dehydrated Na-RUB-29 at 673 K without consideration of superstructure problems.

### 3.3. Structure refinements with neutron powder diffraction data

Rietveld refinements of dehydrated Na-RUB-29 at 673 K were carried out first by fitting HRNPD profile with Le Bail intensity extraction, where zero point, cell parameters and peak-shape functions were refined simultaneously. The HRNPD pattern of dehydrated Na-RUB-29 was indexed in space group $I222$ with $a = 11.1560(6)$ Å, $b = 17.3965(9)$ Å, $c = 23.888(1)$ Å, and unit cell volume of 4636.0(5) Å$^3$.

Rietveld refinements were performed by stepwise including atomic parameters of O, Si, and Cs, where geometrical constrains $d(\text{Si–O}) = 1.61 \pm 0.01$ Å were applied as additional information about the framework. Group-specific atomic displacement parameters (ADPs) for all O and Si were refined with occupancy factors = 1, while individual isotropic ADPs for Cs1, Cs2, and Cs3 sites (Table 2) were calculated initially with the occupancies fixed to 1, based on the starting model derived from the structural analysis with XSD data mentioned above. The subsequent difference Fourier calculation allowed finding six unique positions suitable for Li and another group of four unique sites in 10 MR-channels (Table 2). The latter could be assigned to sodiums, based on their crystal-chemically reasonable distances to framework oxygens [5] (Table 3). Short interatomic distances 2.7–3 Å between Na3 and Na3 and between Na3 and Na4, as well as between Na1 and Cs3 (Table 3) indicate static disorder at these sites. As shown Figs. 8 and 9, continuously distributed scattering length densities around the sites for Li and Na were observed, except for the site Na1.

In the subsequent refinement cycle applying additional constraints $d(\text{Li–O}) = 2.0 \pm 0.02$ Å, occupancies of the Cs, Na, and Li sites were refined. The final stages of Rietveld analysis included simultaneous refinements of atomic parameters for all framework and non-framework constituents along with isotropic atomic displacements and occupancies of all Cs, Na, and Li sites. The final Rietveld-refinement resulted in the following overall discrepancy indices: $wR_p = 0.0334$ and $\chi^2 = 1.629$ [$wR_p = (M/\Sigma w I_o^2)^{0.5}$ with $M = \Sigma w(I_o - I_c)^2$; $\chi^2 = M/(N-P)$, where $N$ is the number of observations (=3128), and $P$ the number of free variables (=148)]. The good agreement of neutron powder patterns of the calculated model with the observed ones is obvious from Figs. 10a to b. The final structural model is consistent with an idealized structural formula of $Cs_8Na_8Li_{40}Si_{72}O_{172}$ within the standard deviations of occupancy parameters. The refined atomic parameters and selected interatomic distances for framework and non-framework constituents are given in Tables 2 and 3, respectively. The arrangement of the entire structural constituents is illustrated in Figs. 11a–c, and details of the local configurations of extraframework Ca and Na cations are displayed in Fig. 12.

The six different Li sites (Li1–Li6) are located within the $Li_2O$-layers (Fig. 11c), i.e. five unique [$LiO_4$]-tetrahedra (i.e. the sites Li1–Li4, and Li6) and one [$LiO_3$]-moiety (the site Li5). There are 40 Li atoms statistically distributed over the entire 44 interstitials of $Li_2O$-layers per unit cell of this dehydrated Na-RUB29 (Table 2). After all, through the $Na^+$-exchanging task performed in this study, eight Na cations could be substituted for six Cs and two non-framework Li cations. The Na content is a little bit lower than that in another Na-RUB-29 sample ($Cs_6Na_{10}Li_{40}Si_{72}O_{172}$) prepared in a longer exchanging time in the previous study [6]. As same as in dehydrated RUB-29 ($Cs_{14}Li_{42}Si_{72}O_{172}$) at 473 and 673 K [2], no extra sites for Li

Table 2
Fractional atomic coordinates, occupancies, isotropic displacement parameters ($U_{iso}$), and site multiplicity ($M$) of a Na-exchanged, dehydrated form of RUB-29 at 673 K (space group: $I222$; lattice parameter: $a = 11.1560(6)$ Å, $b = 17.3965(9)$ Å, $c = 23.888(1)$ Å; unit cell volume = 4636.0(5) Å$^3$)

| Site | Atom | $X$ | $Y$ | $Z$ | Occupancy | $U_{iso}$ [Å$^2$] | $M$ |
|---|---|---|---|---|---|---|---|
| Si1 | Si | 0.362(1) | 0.506(1) | −0.3469(5) | 1 | 0.010(1) | 8 |
| Si2 | Si | −0.242(2) | 0.413(1) | −0.1260(8) | 1 | 0.010(1) | 8 |
| Si3 | Si | 0.135(2) | 0.277(1) | 0.066(1) | 1 | 0.010(1) | 8 |
| Si4 | Si | 0.003(3) | 0.3007(8) | 0.3253(6) | 1 | 0.010(1) | 8 |
| Si5 | Si | 0.258(2) | 0.346(1) | 0.3527(8) | 1 | 0.010(1) | 8 |
| Si6 | Si | −0.241(2) | 0.585(1) | −0.1171(8) | 1 | 0.010(1) | 8 |
| Si7 | Si | 0.257(2) | 0.658(1) | 0.3524(9) | 1 | 0.010(1) | 8 |
| Si8 | Si | −0.499(3) | 0.6263(8) | −0.1439(5) | 1 | 0.010(1) | 8 |
| Si9 | Si | −0.139(2) | 0.276(1) | 0.064(1) | 1 | 0.010(1) | 8 |
| O1 | O | 0.347(1) | 0.495(1) | 0.2803(5) | 1 | 0.028(1) | 8 |
| O2 | O | −0.002(2) | 0.2592(9) | 0.0812(6) | 1 | 0.028(1) | 8 |
| O3 | O | 0.017(2) | 0.286(1) | 0.2587(6) | 1 | 0.028(1) | 8 |
| O4 | O | −0.201(1) | 0.497(1) | −0.1075(7) | 1 | 0.028(1) | 8 |
| O5 | O | −0.204(3) | 0.384(1) | −0.1862(9) | 1 | 0.028(1) | 8 |
| O6 | O | 0.015(3) | 0.2197(7) | 0.3594(7) | 1 | 0.028(1) | 8 |
| O7 | O | 0.280(3) | 0.277(1) | 0.396(1) | 1 | 0.028(1) | 8 |
| O8 | O | 0.219(3) | 0.215(1) | 0.096(1) | 1 | 0.028(1) | 8 |
| O9 | O | −0.211(3) | 0.609(1) | −0.1804(9) | 1 | 0.028(1) | 8 |
| O10 | O | −0.148(1) | 0.2558(9) | −0.001(1) | 1 | 0.028(1) | 8 |
| O11 | O | −0.384(2) | 0.409(1) | −0.113(1) | 1 | 0.028(1) | 8 |
| O12 | O | 0 | 0 | 0.132(9) | 1 | 0.028(1) | 4 |
| O13 | O | 0.319(3) | 0.314(1) | 0.2960(9) | 1 | 0.028(1) | 8 |
| O14 | O | −0.382(2) | 0.603(1) | −0.107(1) | 1 | 0.028(1) | 8 |
| O15 | O | 0.322(3) | 0.682(1) | 0.295(1) | 1 | 0.028(1) | 8 |
| O16 | O | −0.175(2) | 0.365(1) | 0.069(1) | 1 | 0.028(1) | 8 |
| O17 | O | 0.115(2) | 0.649(1) | 0.340(1) | 1 | 0.028(1) | 8 |
| O18 | O | −0.168(2) | 0.365(1) | −0.081(1) | 1 | 0.028(1) | 8 |
| O19 | O | 0.113(2) | 0.351(1) | 0.349(1) | 1 | 0.028(1) | 8 |
| O20 | O | 0.297(2) | 0.426(1) | 0.3826(9) | 1 | 0.028(1) | 8 |
| O21 | O | −0.492(3) | 0.605(7) | −0.2090(5) | 1 | 0.028(1) | 8 |
| O22 | O | 0.310(2) | 0.576(1) | 0.3699(9) | 1 | 0.028(1) | 8 |
| Li1 | Li | −0.5 | 0.5 | −0.240(1) | 1.0(1) | 0.02(1) | 4 |
| Li2 | Li | 0.340(3) | 0.397(2) | 0.239(1) | 0.6(2) | 0.02(1) | 8 |
| Li3 | Li | −0.326(3) | 0.595(1) | −0.241(1) | 1.0(1) | 0.02(1) | 8 |
| Li4 | Li | 0.003(3) | 0.182(1) | 0.228(1) | 1.0(1) | 0.02(1) | 8 |
| Li5 | Li | −0.143(3) | 0.700(1) | −0.222(2) | 1.0(1) | 0.02(1) | 8 |
| Li6 | Li | −0.189(3) | 0.291(1) | −0.234(2) | 0.8(1) | 0.02(1) | 8 |
| Cs1 | Cs | 0 | 0.5 | 0 | 1.0(1) | 0.03(1) | 2 |
| Cs2 | Cs | −0.5 | 0.5 | 0 | 1.0(1) | 0.12(3) | 2 |
| Cs3 | Cs | 0 | 0.5 | 0.760(2) | 0.9(1) | 0.09(2) | 4 |
| Na1 | Na | 0.5 | 0 | 0.134(3) | 0.6(1) | 0.04(3) | 4 |
| Na2 | Na | 0.0 | 0 | 0 | 0.6(1) | 0.2(1) | 2 |
| Na3 | Na | 0.5 | 0.077(6) | 0 | 0.5(1) | 0.1(1) | 4 |
| Na4 | Na | 0.5 | −0.23(12) | 0 | 0.4(1) | 0.2(1) | 4 |

Table 3
Selected interatomic distances ($d$) and angles ($\angle$) in the structure of dehydrated Na-RUB-29 at 673 K

| Atom1_Atom2 | $d$ [Å] | Atom1_Atom2_Atom3 | $\angle$ [deg] |
|---|---|---|---|
| Si1_O1 | 1.60(1) | O1_Si1_O12 | 114(1) |
| Si1_O12 | 1.62(1) | O1_Si1_O20 | 119(2) |
| Si1_O20 | 1.64(1) | O1_Si1_O22 | 107(2) |
| Si1_O22 | 1.63(1) | O12_Si1_O20 | 108(1) |
| | | O12_Si1_O22 | 100(1) |
| | | O20_Si1_O22 | 108(1) |
| Si2_O4 | 1.61(1) | O4_Si2_O5 | 118(2) |
| Si2_O5 | 1.58(1) | O4_Si2_O11 | 106(1) |
| Si2_O11 | 1.61(1) | O4_Si2_O18 | 98(2) |
| Si2_O18 | 1.60(1) | O5_Si2_O11 | 115(2) |
| | | O5_Si2_O18 | 108(2) |
| | | O11_Si2_O18 | 111(2) |
| Si3_O2 | 1.60(1) | O2_Si3_O8 | 109(2) |
| Si3_O8 | 1.61(1) | O2_Si3_O10 | 106(2) |
| Si3_O10 | 1.60(1) | O2_Si3_O18 | 110(2) |
| Si3_O18 | 1.61(1) | O8_Si3_O10 | 103(2) |
| | | O8_Si3_O18 | 114(2) |
| | | O10_Si3_O18 | 115(2) |
| Si4_O3 | 1.62(1) | O3_Si4_O6 | 110(1) |
| Si4_O6 | 1.63(1) | O3_Si4_O17 | 112(2) |
| Si4_O17 | 1.62(1) | O3_Si4_O19 | 111(2) |
| Si4_O19 | 1.61(1) | O6_Si4_O17 | 115(2) |
| | | O6_Si4_O19 | 103(2) |
| | | O17_Si4_O19 | 105(1) |
| Si5_O7 | 1.61(1) | O7_Si5_O13 | 103(2) |
| Si5_O13 | 1.62(1) | O7_Si5_O19 | 103(2) |
| Si5_O19 | 1.62(1) | O7_Si5_O20 | 108(2) |
| Si5_O20 | 1.61(1) | O13_Si5_O19 | 113(2) |
| | | O13_Si5_O20 | 124(2) |
| | | O19_Si5_O20 | 105(2) |
| Si6_O4 | 1.61(1) | O4_Si6_O9 | 109(2) |
| Si6_O9 | 1.60(1) | O4_Si6_O14 | 115(2) |
| Si6_O14 | 1.62(1) | O4_Si6_O16 | 106(2) |
| Si6_O16 | 1.61(1) | O9_Si6_O14 | 107(2) |
| | | O9_Si6_O16 | 116(2) |
| | | O14_Si6_O16 | 104(2) |
| Si7_O8 | 1.60(1) | O8_Si7_O15 | 115(2) |
| Si7_O15 | 1.60(1) | O8_Si7_O17 | 112(2) |
| Si7_O17 | 1.62(1) | O8_Si7_O22 | 107(2) |
| Si7_O22 | 1.61(1) | O15_Si7_O17 | 108(2) |
| | | O15_Si7_O22 | 106(2) |
| | | O17_Si7_O22 | 109(2) |
| Si8_O6 | 1.63(1) | O6_Si8_O11 | 115(2) |
| Si8_O11 | 1.62(1) | O6_Si8_O14 | 99(2) |
| Si8_O14 | 1.62(1) | O6_Si8_O21 | 106(1) |
| Si8_O21 | 1.60(1) | O11_Si8_O14 | 108(1) |
| | | O11_Si8_O21 | 113(2) |
| | | O14_Si8_O21 | 116(2) |
| Si9_O2 | 1.60(1) | O2_Si9_O7 | 107(2) |
| Si9_O7 | 1.60(1) | O2_Si9_O10 | 106(2) |
| Si9_O10 | 1.60(1) | O2_Si9_O16 | 113(2) |
| Si9_O16 | 1.62(1) | O7_Si9_O10 | 114(2) |
| | | O7_Si9_O16 | 112(2) |
| | | O10_Si9_O16 | 105(2) |
| Li1_O1 (2 ×) | 1.97(2) | O1_Li1_O1 | 121(2) |
| Li1_O21 (2 ×) | 1.97(1) | O1_Li1_O21 | 101(1) |
| | | O1_Li1_O21 | 100(1) |
| | | O1_Li1_O21 | 100(1) |
| | | O1_Li1_O21 | 101(1) |
| | | O21_Li1_O21 | 136(2) |
| Li2_O1 | 1.99(2) | O1_Li2_O5 | 117(2) |
| Li2_O5 | 1.95(2) | O1_Li2_O13 | 106(2) |
| Li2_O13 | 1.98(2) | O1_Li2_O21 | 99(1) |
| Li2_O21 | 2.01(2) | O5_Li2_O13 | 105(2) |
| | | O5_Li2_O21 | 119(2) |
| | | O13_Li2_O21 | 110(2) |
| Li3_O1 | 1.99(2) | O1_Li3_O9 | 122(2) |
| Li3_O9 | 1.95(2) | O1_Li3_O15 | 111(2) |
| Li3_O15 | 1.98(2) | O1_Li3_O21 | 98(1) |
| Li3_O21 | 2.01(2) | O9_Li3_O15 | 112(1) |
| | | O9_Li3_O21 | 108(2) |
| | | O15_Li3_O21 | 102(2) |
| Li4_O3 | 1.96(2) | O3_Li4_O13 | 98(1) |
| Li4_O13 | 2.13(2) | O3_Li4_O15 | 92(1) |
| Li4_O15 | 2.03(2) | O3_Li4_O21 | 109(1) |
| Li4_O21 | 2.02(2) | O13_Li4_O15 | 149(1) |
| | | O13_Li4_O21 | 104(2) |
| | | O15_Li4_O21 | 100(2) |
| Li5_O3 | 2.00(2) | O3_Li5_O9 | 130(2) |
| Li5_O9 | 2.02(2) | O3_Li5_O13 | 99(1) |
| Li5_O13 | 2.07(2) | O9_Li5_O13 | 125(2) |
| Li5_O15 | 2.66(6) | | |
| Li6_O3 | 2.01(2) | O3_Li6_O5 | 107(2) |
| Li6_O5 | 1.98(2) | O3_Li6_O13 | 117(2) |
| Li6_O13 | 2.13(2) | O3_Li6_O15 | 90(1) |
| Li6_O15 | 2.02(2) | O5_Li6_O13 | 101(2) |
| | | O5_Li6_O15 | 126(2) |
| | | O13_Li6_O15 | 117(2) |
| Li1_Li2 | 2.53(3) | | |
| Li1_Li3 | 2.55(3) | | |
| Li1_Li4 | 3.26(2) | Li3_Li6 | 3.46(4) |
| Li2_Li3 | 3.45(3) | Li4_Li5 | 2.62(4) |
| Li2_Li4 | 2.42(5) | Li4_Li6 | 2.80(3) |
| Li2_Li6 | 2.50(4) | Li5_Li6 | 2.67(5) |
| Li3_Li4 | 2.55(4) | | |
| Li3_Li5 | 2.77(5) | | |
| Cs1_O4 ( × 4) | 3.41(2) | Cs1_Cs2 | 5.5780(3) |
| Cs1_O16 ( × 4) | 3.47(3) | Cs1_Cs3 | 5.74(4) |
| Cs1_O18 ( × 4) | 3.58(3) | | |
| Cs2_O11 ( × 8) | 3.39(3) | | |
| Cs3_O1 ( × 2) | 3.98(2) | | |
| Cs3_O3 ( × 2) | 3.75(2) | | |
| Cs3_O4 ( × 2) | 3.88(3) | | |
| Cs3_O5 ( × 2) | 3.31(4) | | |
| Cs3_O9 ( × 2) | 3.35(4) | | |
| Cs3_O17 ( × 2) | 3.74(3) | | |
| Cs3_O19 ( × 2) | 3.89(4) | Na1_Cs3 | 3.00(8) |
| | | Na1_Na3 | 3.47(8) |
| Na1_O17 ( × 2) | 2.96(3) | Na3_Na3 | 2.7(2) |
| Na1_O19 ( × 2) | 2.92(3) | Na3_Na4 | 2.7(2) |
| Na2_O12 ( × 2) | 3.16(2) | Na4_Cs2 | 4.7(2) |

could be found in 8- and 10-MR channels of Na-RUB-29 at 673 K. The remaining six non-framework Li cations in the channel system [1], which were not exchanged by $Na^+$, might have migrated into $Li_2O$-layers upon dehydration. This is further indication that non-framework Li cations prefer to be within the $Li_2O$-layers when there is no zeolitic water [2].

As a result of this $Na^+$-exchange process, however, the number of migrating channel Li cations in Na-RUB-29 is

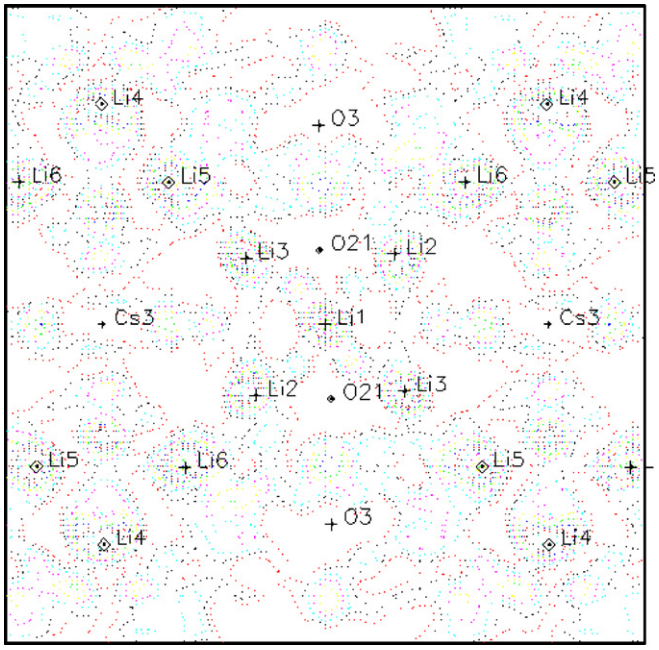


Fig. 8. Section ($x$, $y$, 0.23) of difference Fourier-map from HRNPD data of Na-RUB-29 at 673 K. Six different negative maxima Li1–Li6 are surrounded by continuous scattering length densities (Center of reference: 0.5, 0.5, 0.23; height above the center: 0 Å; contours are drawn between −9.75 and −0.65).

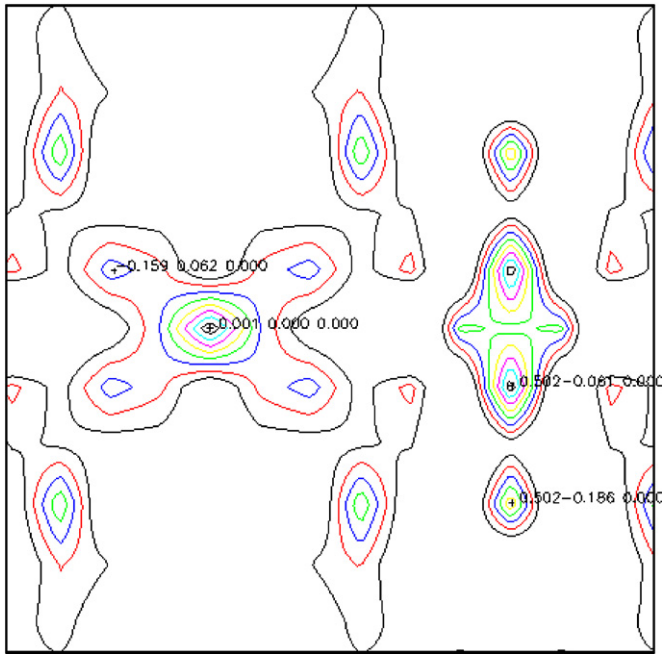


Fig. 9. Section (0.2, $y$, $z$) of difference Fourier-map from HRNPD data of Na-RUB-29 at 673 K. Differently strong positive maxima confined by continuous scattering length densities could be assigned to the positions suitable for statically and dynamically disordered Na cations (Center of reference: 0.2, 0.0, 0.0; height above the center: 0 Å; contours are drawn between 0.6 and 4.8).

less than that in RUB-29. This means that the degree of availability for optimal pathways for hopping $Li^+$ in the RUB-29 topology, i.e. the empty sites in $Li_2O$-layers, can be improved by $Na^+$-exchanging. In the presence of empty Li sites within the $Li_2O$-layers, local site-exchanging processes between directly neighboring edge-sharing $LiO_4$-tetrahedra (Fig. 11c) can readily occur, which, in turn, promotes the long-range $Li^+$ conduction. This may be one of the main reasons for the shift of the HF′ to higher frequencies and the high conductivity in $Na^+$-exchanged RUB-29 samples.

The difference between the empty sites within the $Li_2O$-layers of Na-RUB-29 and those of RUB-29 is small, i.e. four and two per unit cell, respectively. On the other hand, the observation of continuous scattering length densities around Na positions suggests further searching for structural basis of the improved conductivity in Na-RUB-29. All three sites Cs1, Cs2, and Cs3 refined as being occupied by Cs (Figs. 12a–c) show almost 100% occupation (Table 2). However, compared to Cs1, the Cs2 and Cs3 sites present very large ADPs parameters. This could be caused by two factors: first, at Cs2 and Cs3 sites, both Cs and Na would be statically disordered. Then, the averaged atomic parameters of Cs2 and Cs3 are uncertain with a high correlation of ADPs with occupancy parameters; second, it could be due to dynamic disorder of Cs, if this species would occupy both Cs2 and Cs3 sites alone. However, the first case, i.e. static disorder of Cs and Na at Cs2 and Cs3 seems to be unlikely in this compound, as Rietveld calculations of the fractions of Cs and Na with constraints of 100% occupations of each site by both Na and Cs resulted in nearly zero occupancies of Na for Cs2 and Cs3 sites. In this respect, the site Na1 which was refined as a partially occupied site for Na alone (60%, Table 2) might be occupied by both Na and Cs. This, taking the smaller coherent scattering length of Na ($=3.63\times10^{-15}$ m) than that of Cs ($=5.42\times10^{-15}$ m) into consideration, is due to the fact that the sum of the occupancy parameters of Na1 and Cs3 lies higher than 100%.

With these features, we consider dynamic disorder of Cs cations as the main reason for the high ADPs for Cs2 and Cs3 sites. Cs cations can move more freely at spacious Cs2 and Cs3 sites than within the tight Cs1 site. The condition for dynamic motions of Cs cations seems to be limited at the site Cs1, as this is included within a small cage-like pore space bounded by four 8 MRs and two 4 MRs of $SiO_4$-tetrahedra (Fig. 12a). In this geometrical condition, the interaction between charge-balancing $Cs^+$ and the electrostatically negative-charged lithosilicate framework might be high. In fact, it was figured out that the bond valence of $Cs^+$ [16,17] was highest at Cs1 among seven positions available for Cs cations in the original RUB-29 structure [18].

However, beside the fast Li motions, one of the main reasons for the HF′ relaxation processes might be attributed rather to cationic motions within much larger pores, than to those at Cs2 and Cs3. This is simply due to the fact that Cs2 and Cs3 are occupied by Cs cations not only in Na-RUB-29, but also in RUB-29. The

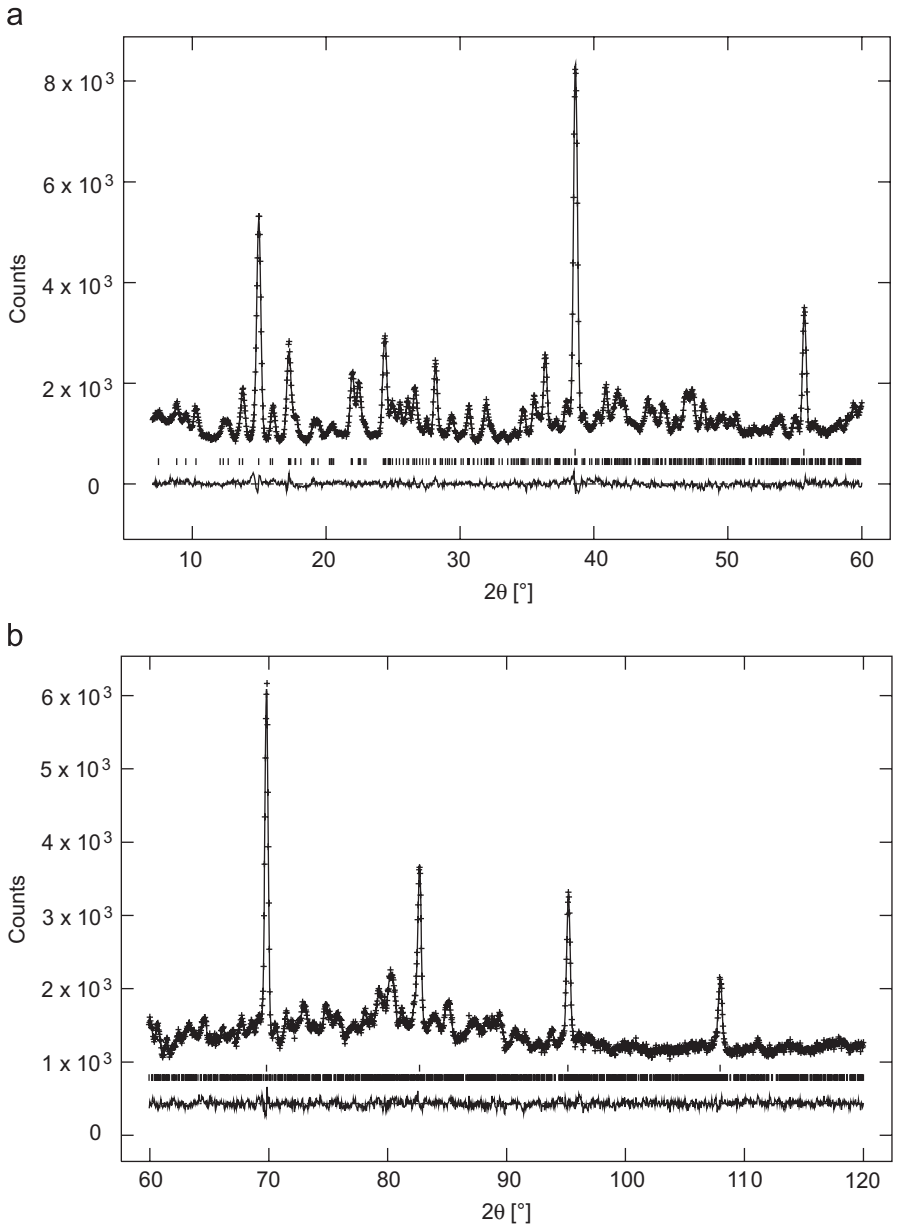


Fig. 10. Calculated (line) and observed (crosses) neutron powder diffraction pattern of dehydrated Na-RUB-29 at 673 K presented in two $2\theta$ ranges: 7–60 ° (a) and 60–120° (b). The upper and lower tick marks indicate reflections of the Nb sample can and Na-RUB-29, respectively. The lower curve shows the difference between the observed and calculated data.

$Na^+$-substitution occurred predominately for those Cs cations located in the intersection points of two 10 MR-channels, such as the sites Na2–Na4 (Fig. 12e), and then at the other spacious positions, such as Na1 (Fig. 12d). The sites Na2–Na4 show very large isotropic ADPs compared to that of Na1 (Table 2). Like Cs1, the site Na1 is located within less porous space in comparison to the rest Na sites. For this reason, Na cations at Na1 cannot be as highly mobile as those at Na2–Na4. Furthermore, it is more than a coincidence to observe continuous scattering length densities clearly seen around the sites Na2, Na3, and Na4 in difference Fourier maps (Fig. 9), but not the case for the site Na1.

At these most porous spaces Na2–Na4 in this topology, motions of smaller $Na^+$ can be higher than those of bulky $Cs^+$. This can explain why the HF′ relaxation frequency became so high after $Na^+$-exchanging and shifted out of the measuring frequency region already above 543 K. Now it is more clear that, among all $Cs^+$ in dehydrated RUB-29, those Cs cations mobile within intersections of two 10 MR-channels are highly involved in the HF′ relaxation processes.

In conclusion, the structural investigation of a high-temperature form of Na-RUB-29 at 673 K helped to explain the high conductivity due to short- and long-range hopping of framework Li cations and motions of

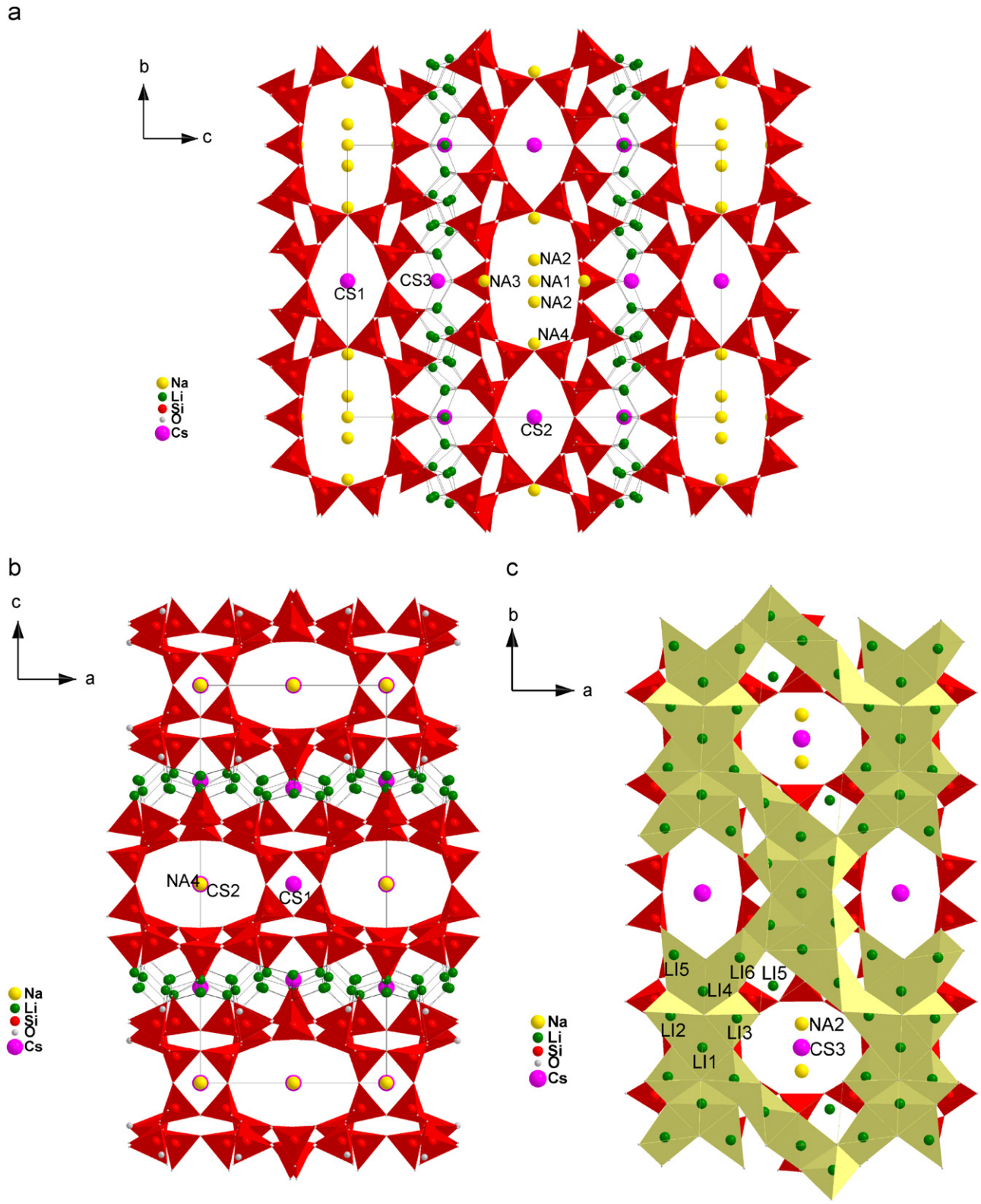


Fig. 11. Structure of dehydrated Na-RUB-29, projected along [1 0 0]- (a), [0 1 0]- (b), and [0 0 1]-direction (c). In Fig. 11c, the framework is presented by [$LiO_4$]- and [$SiO_4$]-tetrahedra in bright and dark tone, respectively.

$Na^+$. This study reports a high overall conductivity value of $3.2 \times 10^{-3}\,S\,cm^{-1}$ for Na-RUB-29 ($Cs_8Na_8Li_{40}Si_{72}O_{172}$) at 885 K, and therefore confirms the high conductivity value of $7 \times 10^{-3}\,S\,cm^{-1}$ for another Na-RUB-29 variant ($Cs_6Na_{10}Li_{40}Si_{72}O_{172}$). The latter shows a slightly higher content of Na and higher conductivity. The proportionality of the overall conductivity to the degree of $Na^+$-incorporation into RUB-29 and a careful comparison with

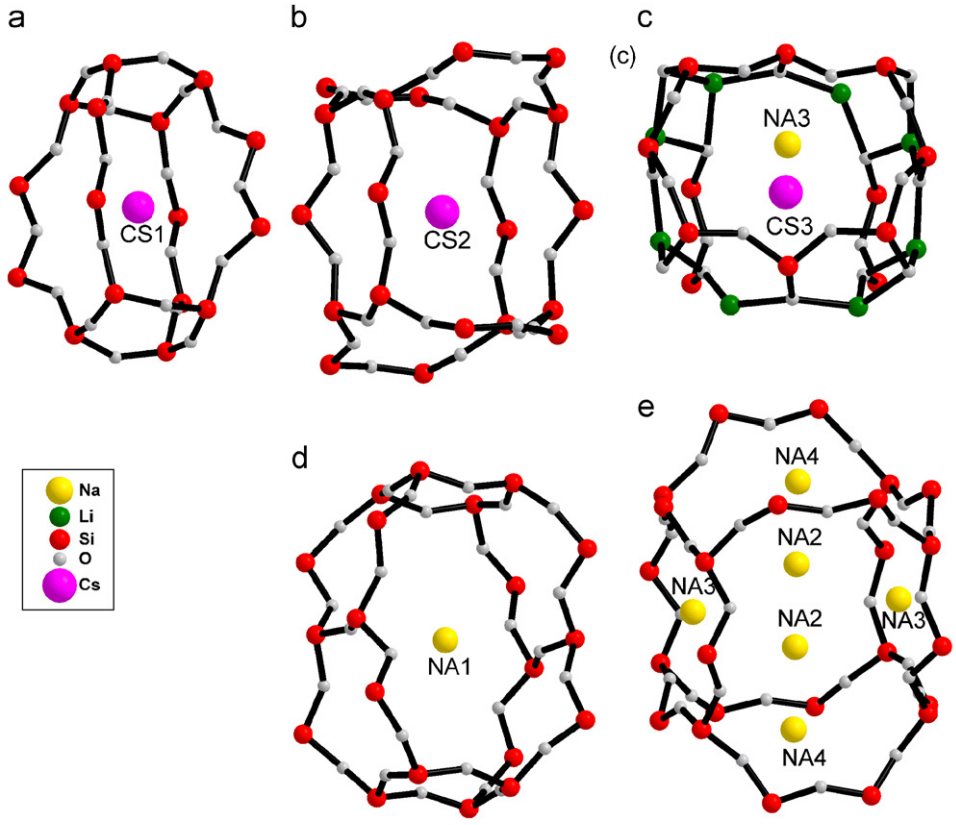


Fig. 12. Local configuration of the sites for Cs and Na cations in dehydrated Na-RUB-29. The sizes of all species presented here do not correspond to their real physical sizes.

IS spectra of dehydrated RUB-29 allow a relevant conclusion: the HF′ relaxation processes can be assigned to fast dynamic disorder of both $Li^+$ within $Li_2O$-layers and $Na^+$ (or $Cs^+$ before $Na^+$-exchanging) within most porous intersections of 10 MR-channels. The conductivity values of Na-RUB-29 materials reach in the highest region ever observed in zeolitic cationic conductors, so far [11,14,19]. This is accordance with observations that among zeolitic materials $Na^+$-exchanged ones show highest ionic conductivity [11,14,19].

The present work showed a special situation for an indirect tuning of empty framework Li sites via 'simple' $Na^+$-exchange processes. The configuration and type of non-framework cations can greatly influence the dynamic and static disorder of framework $Li^+$ in the RUB-29 topology. This implication will be further verified by studying various cation-exchanged RUB-29-type materials.

## Acknowledgments

SHP acknowledges financial support from the DFG via PA 1222/1-2. We thank Dr. Elmar Schmidbauer for support in conducting impedance measurements at LMU.

## References

[1] S.-H. Park, J.B. Parise, H. Gies, H. Liu, C.P. Grey, B.H. Toby, J. Am. Chem. Soc. 122 (2000) 11023–11024.
[2] S.-H. Park, J.B. Parise, M.E. Franke, T. Seydel, C. Paulmann, Micropor. Mesopor. Mater., in press (doi:10.1016/j.micromeso2007.03.040 available online since April 19, 2007).
[3] S.-H. Park, P. Daniels, H. Gies, Micropor. Mesopor. Mater. 37 (2000) 129–143.
[4] S.-H. Park, J.B. Parise, H. Gies, Studies in Surface Science and Catalysis, vol. 135, Elsevier, Amsterdam, Paper 09-0-05, 2001.
[5] R.D. Shannon, Acta Crystallogr. A 32 (1976) 751–769.
[6] M.E. Franke, L. Rodriguez-Gonzalez, U. Simon, S.-H. Park, Abstracts of 16th Deutsche Zeolith-Tagung, Dresden, Germany, March 3–5, 2004.
[7] S.-H. Park, F. Frey, C. Paulmann, Abstract #041-06, Annual meeting of DGK (Deutsche Gesellschaft für Kristallographie), Bremen, Germany, March 5–8, 2007.
[8] W.J. Kabsch, J. Appl. Crystallogr. 26 (1993) 795–800.
[9] M.A. Estermann, W. Steurer, Phase Transit 67 (1996) 165–195.
[10] A.C. Larson, R.B. Von Dreele, GSAS (General Structural Analysis System), Los Alamos National Laboratory Report LAUR 86-748, Los Alamos National Laboratory, Los Alamos, NM, USA, 2000.
[11] U. Simon, M.E. Franke, Micropor. Mesopor. Mater. 41 (2000) 1–36.
[12] J.R. Macdonald, Impedance Spectroscopy, Wiley, New York, 1987.
[13] Y.T. Tsai, D.H. Whitmore, Solid State Ion. 7 (1982) 129–139.
[14] G. Kelemen, W. Lortz, G. Schön, J. Mater. Sci. 24 (1989) 333–338.
[15] U. Simon, U. Flesch, J. Porous Mater. 6 (1999) 33–40.
[16] I.D. Brown, in: M.O'. Keeffe, A. Navrotsky (Eds.), Structures and Bonding in Crystals, Academic Press, New York, 1981 (Chapter 14).
[17] I.D. Brown, R.D. Shannon, Acta Crystallogr. A 29 (1973) 266–282.
[18] S.-H. Park, M. Kleinsorge, C.P. Grey, J.B. Parise, J. Solid State Chem. 167 (2002) 310–323.
[19] G. Kelemen, G. Schön, J. Mater. Sci. 27 (1992) 6036–6040.